FULL PAPER

Dalton
www.rsc.org/dalton

Synthesis, structure and magnetism of new single molecule magnets composed of $Mn^{II}_2Mn^{III}_2$ alkoxo-carboxylate bridged clusters capped by triethanolamine ligands †

Lisa M. Wittick,[a] Keith S. Murray,*[a] Boujemaa Moubaraki,[a] Stuart R. Batten,[a] Leone Spiccia[a] and Kevin J. Berry[b]

[a] *School of Chemistry, Monash University, Victoria, 3800, Australia. E-mail: keith.murray@sci.monash.edu.au; Fax: 61 3 9905 4597; Tel: 61 3 9905 4512*

[b] *Westernport Secondary College, Hastings, Victoria, 3915, Australia*

Received 10th October 2003, Accepted 18th February 2004
First published as an Advance Article on the web 2nd March 2004

A family of tetranuclear mixed-valent $Mn(II)_2/Mn(III)_2$ complexes of type $[Mn_4(LH_2)_2(LH)_2(H_2O)_x(RCO_2)_2](Y)_2{\cdot}nS$ has been synthesised and structurally characterised, where LH_3 = triethanolamine ($N(CH_2CH_2OH)_3$), {R = CH_3, x=2, Y = $CH_3CO_2^-$, n=2, S = H_2O; **1**}, {R = C_6H_5, x=0, Y = $C_6H_5CO_2^-$, n=1, S = CH_3CN; **2**}, {R = C_2H_5, x=0, Y = ClO_4^-, n=0; **3**}. A common structural core was deduced from X-ray crystallography and consists of a rhomboidal (planar-diamond) array with two 7-coordinate Mn(II) 'wingtip (w)' centres and two 6-coordinate Mn(III) 'body (b)' centres. The Mn(III) ions are bridged to the Mn(II) ions by μ_3-oxygen atoms from a deprotonated alcohol 'arm' of each tridentate LH^{2-} ligand and by μ_2-oxygen atoms from each tetradentate LH_2^- ligand. The four nitrogen atoms from LH^{2-} and LH_2^- groups, together with bridging and terminal carboxylates oxygens complete the outer coordination sites around the Mn atoms. A feature of these clusters is that they are linked together in the crystal lattice by hydrogen-bonding interactions involving a non-coordinated hydroxyl arm on each LH^{2-} group. Detailed DC and AC magnetic susceptibility measurements and magnetisation isotherms have been made on the three complexes and show that intra-cluster ferromagnetic coupling is occurring between the S=2 Mn(III) and S=5/2 Mn(II) ions to yield S=9 ground states. The g, J_{bb} and J_{wb} parameters have been deduced. Inter-cluster antiferromagnetic coupling was noted in **3** and this influences the magnetisation *versus* field behaviour and the temperature and magnitude of the out-of-phase AC χ''_M maxima in comparison to those observed for **1** and **2**. An Arrhenius plot of the reciprocal temperature of the maxima in χ''_M obtained at different frequencies (10 to 1500 Hz), in the range 1.75 K to 4 K, against the natural logarithm of the magnetization relaxation rate ($1/\tau$) yielded values of the activation energies and pre-exponential factors for two of these new tetranuclear single-molecule magnets (SMMs), **1** and **2**. The activation energies were compared with the potential energy barrier height, U, for magnetisation direction reversal ($U = DS^2$) using the axial zero-field splitting parameter, D, deduced from the DC M/H isotherm analysis for these S=9 species. The very small separation of S=9 and 8 levels for these clusters highlights the limitations in the determination of D values from M/H data at low temperatures.

Introduction

Our studies of manganese clusters, including those of the single molecule magnet (SMM) type, grew out of attempts to make extended networks of small clusters, such as of the trinuclear Mn_3O carboxylate or of the Mn_4O_2 'butterfly' units, by use of bridging ligands of the dicyanamide and tricyanomethanide types. We had preliminary results that such networks could be formed by tethering $Ni_4(OR)_4$ cubane units together.[1] In the manganese chemistry, no such networks have been obtained thus far,‡ but, rather some medium sized mixed-valent Mn_4 (non-SMM) and large Mn_{16} SMM examples.[2,3] The latter cluster provided a new member of the beautiful array of manganese oxo-carboxylato clusters, of varying molecularity, many displaying the important quantum tunneling properties of SMM molecular clusters, studied in depth by the groups of Christou,[4] Hendrickson,[4] Gatteschi,[5] Sessoli[5] and their coworkers.

Our work is continuing efforts to make nanomagnetic cluster species. At a chemical level, one aim has been to use donor atoms in the 'outer' bridging ligands different than the commonly used O-donors of carboxylate. We have had preliminary success in using isoelectronic amidinates,[6] $RC(NH)(=NH)^-$ and in the use of triethanolamine, $N(CH_2CH_2OH)_3$ (labelled LH_3) which is the topic of this paper, a ligand which forms alkoxo, OR^-, bridges within the core of tetranuclear $Mn(II)_2Mn(III)_2$ clusters and uses the N donor in some of the outer coordination positions. Contemporaneous with this work have been related studies of similar clusters by Christou *et al.*[7,8] using 2-hydroxymethylpyridine (Hhmp) or pyridine-2,6-dimethanol ($pdmH_2$) ligands. This group has also employed the tripodal ligand 1,1,1-tris(hydroxymethyl)ethane, $thmeH_3$, to make a Mn_9 SMM containing $\{Mn(IV)_3\ Mn(III)_4\ Mn(II)_2\}$.[9] ‡. These hydroxymethyl ligands have the common feature of being able to coordinate in these clusters in more than one partly deprotonated form and this probably helps to stabilize the products, formed without addition of external base. They can also have coordinated CH_2O^- and coordinated or non-coordinated CH_2OH 'arms'. The family of compounds described in detail here, $[Mn_4(LH_2)_2(LH)_2(H_2O)_2(MeCO_2)_2]$ $(MeCO_2)_2{\cdot}2H_2O$ (**1**), $[Mn_4(LH_2)_2(LH)_2(PhCO_2)_2](PhCO_2)_2{\cdot}MeCN$ (**2**) and $[Mn_4(LH_2)_2(LH)_2(EtCO_2)_2](ClO_4)_2$ (**3**), shows variation in the carboxylate group and in subtle coordination modes around the Mn ions, but with an essentially common core structure. Each complex also exhibits cluster–cluster interactions in the crystalline state, *via* hydrogen bonding. It was of considerable interest to see if such intermolecular effects would influence the SMM intracluster

† Electronic supplementary information (ESI) available: Detailed magnetisation discussion, Mn bond valence sums (Table S1), H-bonding details (Table S2). See http://www.rsc.org/suppdata/dt/b3/b312672b/

‡ *Note added in proof*. A 3D network $[Mn_4(hmp)_4(OH)_2Mn(dca)_6]{\cdot}2MeCN{\cdot}2THF$ has just been published[24] and contains the present type of clusters bridged by dicyanamide (dca^-) to Mn^{II} centres. Inter-cluster ferrimagnetic ordering occurs at 4.1 K with $J_{3D} = -0.02$ cm^{-1}.

An iron(III) triethanolamine cluster $[Fe_8O_3(O_2CPh)_9(L)(LH_3)]$, with ground state S = 0, has also been reported.[25]

DOI: 10.1039/b312672b

magnetic properties and if they would lead to cluster–cluster short- or long-range coupling and/or ordering. Such effects have also been noted recently in the hmp^- and $pdmH^-$ systems by means of very low temperature heat capacity or hysteresis (exchange bias) measurements.[10–12] The SMM behaviour was retained in these systems and we have observed that it is also the case in compounds **1** to **3**.

Experimental

Physical measurements

Elemental analyses (CHN) were carried out by Campbell Microanalytical Laboratory, University of Otago, Dunedin, New Zealand. IR spectra were recorded on a Perkin-Elmer 1600 Series Spectrometer with the samples prepared as KBr discs.

Synthesis

All reactions were carried out under aerobic conditions using commercial grade solvents. Triethanolamine (LH_3; obtained from Ajax Inc.) was used as received without further purification. $[Mn_3O(MeCO_2)_6(py)_3]$, $[Mn_3O(EtCO_2)_6(py)_3](ClO_4)$ and $[Mn_3O(PhCO_2)_6(py)_2(H_2O)]$ were prepared as described elsewhere.[13,14]

$[Mn_4(LH_2)_2(LH)_2(H_2O)_2(MeCO_2)_2](MeCO_2)_2\cdot 2H_2O$ (1). $[Mn_3O(MeCO_2)_6(py)_3]$ (173 mg, 0.20 mmol) was dissolved in MeCN (20 ml) and to this solution was added LH_3 (94 mg, 0.6 mmol). The solution was stirred for 30 min then left to evaporate slowly. After 3 days large red crystals of **1** were collected by filtration and dried in air. Yield 78% (72 mg); IR data (KBr disk, cm^{-1}): 3356s, 2930s, 2867s, 1577s, 1412s, 1386s, 1331s, 1253w,1162w, 1147w, 1089s, 1051m, 1030m, 918m, 888m, 745m, 659m, 606w, 586w, 568w, 515w,480w, 417w. Anal. for $Mn_4C_{32}H_{74}N_4O_{24}$. Calc (%) C, 34.4; H, 6.7; N, 5.0. Found: C, 34.7; H, 6.7; N, 4.9.

$[Mn_4(LH_2)_2(LH)_2(PhCO_2)_2](PhCO_2)_2\cdot CH_3CN$ (2). $[Mn_3O(PhCO_2)_6(py)_2(H_2O)]$ (111 mg, 0.10 mmol) was dissolved in MeCN (20 ml) and to this solution was added tea (48 mg, 0.30 mmol).The solution turned red–brown and was stirred for 30 min. The solution was left and fine red needles of **2** formed after several hours. The crystals were collected by filtration and dried in air. Yield 59% (61 mg); IR data (KBr disk, cm^{-1}): 3357s br, 3063s, 2933s, 2860s, 2146m, 1924w, 1848w, 1831w, 1775w, 1752w, 1719w, 1702w, 1600s, 1579s, 1488w, 1448m, 1381s, 1305m, 1227w, 1173w, 1138w, 1088s, 1069s, 1032m, 915m, 909m, 888m, 831w, 723s, 674m, 644m, 601m, 564m, 513w, 461w, 435w. Anal. for $Mn_4C_{54}H_{77}N_5O_{20}$. Calc (%) C, 48.5; H, 5.8; N, 5.2. Found: C, 47.5; H, 5.6; N, 5.0.

$[Mn_4(LH_2)_2(LH)_2(EtCO_2)_2](ClO_4)_2$ (3). $[Mn_3O(O_2CEt)_6(py)_3](ClO_4)$ (102 mg, 0.1 mmol) was dissolved in MeCN (20 ml) and to this solution was added LH_3 (47 mg, 0.3 mmol). The solution was stirred for 30 min and then evaporated to yield a thick oil. The oil was redissolved in MeOH and layered with Et_2O. After several days grey crystals of **3** were collected by filtration and dried in air. Yield 40% (22 mg); IR data (KBr disk, cm^{-1}): 3380vs br, 3356vs br, 3152s, 2965s, 2934s, 2899s, 2853s, 2344w, 2227w, 1775w, 1702w, 1591s, 1462m, 1450s, 1386s, 1352m, 1325m, 1301m, 1250w, 1230w, 1145s, 1116vs br, 1088vs br, 1027s, 917s, 886m, 745w, 808w, 744w, 627s, 564m, 512m, 458w. Anal. for $Mn_4C_{30}H_{64}N_4O_{24}Cl_2$. Calc (%) C, 31.2; H, 5.6; N, 4.9. Found: C, 31.6; H, 5.6; N, 4.8.

X-ray crystallography

X-Ray crystallographic measurements were performed at 123(2) K using a Nonius Kappa CCD diffractometer, fitted with a Mo-Kα radiation source and graphite monochromator ($\lambda = 0.71073$). DENZO-SMN[15] was used for data integration and SCALEPACK[15] corrected data for Lorentz-polarisation effects. Direct methods (SHELXS 97)[16] and successive Fourier difference methods with refinement of full matrix least squares on F_{obs}^2 (SHELXL 97) afforded structural solutions. For complex **1** all hydrogen atoms were located in the difference maps and allowed to refine freely except for H(14C), H(14D) and H(12), which were restrained to no less than 0.84(1) from the corresponding oxygen atom. Complex **2** was a thin needle and diffracted only weakly, and thus a high R_{int} (0.2482) was obtained. An earlier data set on this compound resulted in an even less satisfactory refinement. Hydrogen atoms were assigned to geometrically idealised positions except for H(2) and H(3) which were located in the difference map and allowed to refine freely and H(8) which was located in the difference map and restrained to no less than 0.84(2) from the corresponding oxygen atom. For complex **3**, hydrogen atoms were assigned to geometrically idealised positions except for H(1A) which was located in the difference map and allowed to refine freely. The hydrogen bonded to O(2) could not be located in the difference map and was not assigned. However, from charge balance considerations, the indication of a hydrogen bond to a neighbouring perchlorate (O ··· O = 2.851(5) Å) and comparisons to the analogous structures, **1** and **2**, it was assumed to be present.

CCDC reference numbers 221593 (**1**), 221594 (**2**) and 221595 (**3**).

See http://www.rsc.org/suppdata/dt/b3/b312672b/ for crystallographic data in CIF or other electronic format.

Magnetic measurements

DC magnetic measurements were carried out on a Quantum Design MPMS 5 SQUID magnetometer calibrated by use of a standard palladium sample (Quantum Design) of accurately known magnetisation or by use of magnetochemical calibrants such as $CuSO_4\cdot 5H_2O$. Susceptibility *vs.* temperature studies in the linear portion of the magnetisation *vs.* field curve were made using a field of 1 T. A powder sample dispersed in vaseline was contained in a calibrated gelatine capsule held at the centre of a drinking straw fixed to the end of the sample rod in order to avoid torquing of the crystallites. Magnetization measurements were made in fields of between 0 and 5 T. AC susceptibilities were made using a Quantum Design PPMS instrument with an AC field of 1 Oe and frequencies varying over the range 10 to 1500 Hz, at temperatures between 1.75 and 4 K.

Results and discussion

Synthesis and constitution

The tetranuclear clusters **1**–**3** were prepared by reacting the appropriate trinuclear μ_3-oxo manganese (III,III,II) carboxylate–pyridinate clusters (for **1** and **2**), in MeCN, with triethanolamine in a 1 : 3 mole ratio. Complex **3** used the (III,III,III) propionate precursor as the ClO_4^- salt in the way used by Christou *et al.* for an acetate/pdmH analogue.[8] The compounds contain mono- and di-deprotonated triethanolamine groups, LH_2^- and LH^{2-}, in the same 2 : 2 ratio, a situation probably influenced by the 'built in' bases RCO_2^- and pyridine. Of the few known Mn triethanolamine compounds, a heptanuclear cluster, $[Mn^{II}_4Mn^{III}_3(LH)_3(L)_3](ClO_4)_2\cdot 3MeOH$, has been found to contain two different levels of deprotonation of triethanolamine.[17] Bond valence sum calculations on **1**–**3** gave excellent agreement with the Mn^{II} and Mn^{III} oxidation states assigned from structures and formulae (Table S1, ESI †).

Support for the formulae and the protonation states of the CH_2CH_2OH arms in the LH^{2-} and LH_2^- forms of the ligand came from the structural analysis (below). All protons were

resolved in **1**, with good thermal parameters, including those on the oxygen atoms of LH_2^- and LH^{2-}. These protons are further confirmed in their H-bonding to H_2O molecules or acetate ions. The ionic and terminally coordinated acetates lacked any residual peaks in the structural analysis and both C–O lengths were very similar, close to C=O values, indicative of being deprotonated. Their involvement in H-bonding to LH_2^- (OH) and water protons also supports their deprotonated formulation. The same situation applies to **2** and **3** (see Experimental section).

Description of structures

Labeled ORTEP plots of **1**, **2** and **3** are given in Figs. 1, 2 and 3. Crystallographic information is given in Table 1 and selected interatomic distances and angles are listed in Table 2.

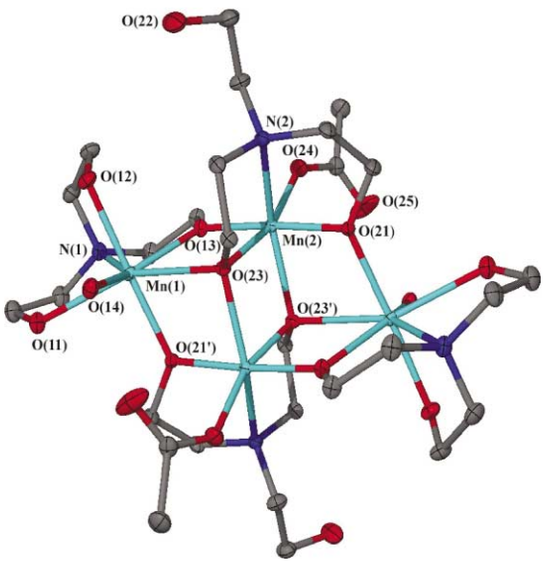

Fig. 1 ORTEP plot of the $[Mn_4(LH_2)_2(LH)_2(H_2O)_2(MeCO_2)_2]^{2+}$ cluster contained in **1**.

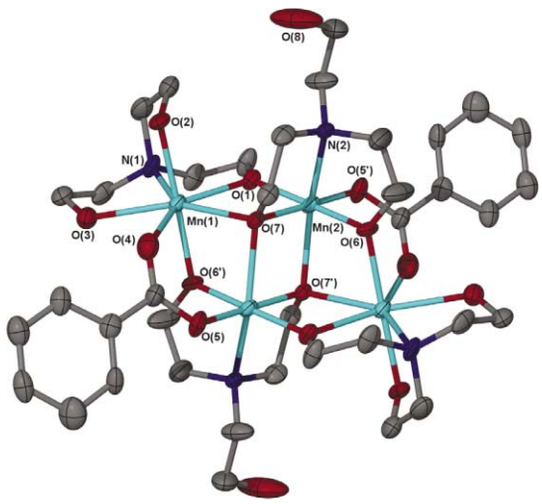

Fig. 2 ORTEP plot of the $[Mn_4(LH_2)_2(LH)_2(PhCO_2)_2]^{2+}$ cluster contained in **2**.

Complex **1** crystallised in the triclinic space group $P\bar{1}$ while complexes **2** and **3** crystallised in the monoclinic space groups $C2/c$ and $P2_1/c$ respectively. The clusters lie on inversion centres relating one half of the molecule to the other with the asymmetric unit containing half the cluster and various counterions and solvent molecules. The core of the clusters is a mixed-valence rhombus held together by two μ_3-O and four μ_2-O with the metals in a roughly planar arrangement. There are four tea ligands present in two different bonding forms [A (LH^{2-}) and B (LH_2^-)] with two of each type present.

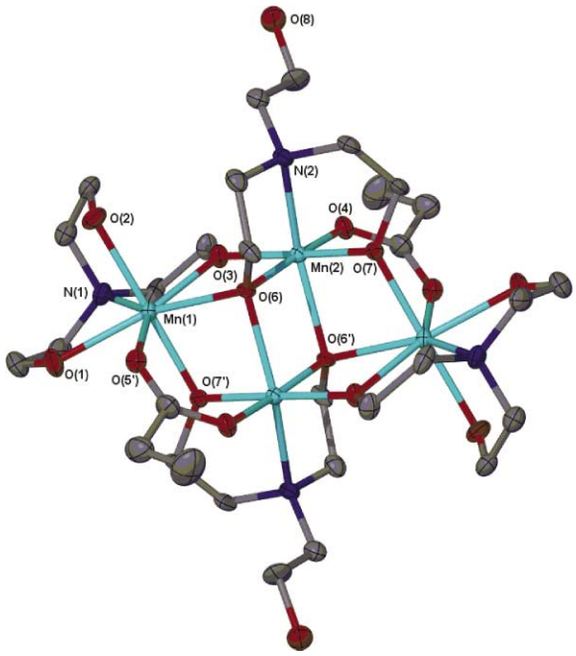

Fig. 3 ORTEP plot of the $[Mn_4(LH_2)_2(LH)_2(EtCO_2)_2]^{2+}$ cluster contained in **3**.

Type A is tridentate with a μ_3-O bridging three metal centres, a μ_2-O bridging two metal centres and the nitrogen terminally coordinated. Both bridging oxygens are deprotonated while the third oxygen is protonated and uncoordinated to any of the metal centres. Type B is tetradentate and possess a deprotonated μ_2-O bridging two Mn centres while the other arms are protonated and terminally coordinated to Mn, as is the nitrogen. Two terminal acetates and two terminal waters complete ligation in complex **1** while complexes **2** and **3** contain two benzoates and propionates respectively that are bidentate and terminally coordinated. Consequently, in all the clusters Mn(1) and Mn(2) are seven- and six-coordinated respectively. Mn(1) has distorted pentagonal bipyramidal geometry while Mn(2) has distorted octahedral geometry. On the basis of structural parameters Mn(1) and Mn(2) were assigned as being Mn^{II} and Mn^{III} respectively. Mn(1) displays longer Mn–ligand bond lengths compared with those for Mn(2), while Mn(2) shows Jahn–Teller distortion in the form of an elongation of one of the axes, as expected for a high-spin d^4 system in near-octahedral geometry.

$[Mn_4(LH_2)_2(LH)_2(H_2O)_2(MeCO_2)_2](MeCO_2)_2\cdot 2H_2O$ (1). The asymmetric unit contains half the cluster, a water molecule and an acetate ion. Mn(1) displays longer Mn–ligand bond lengths (average 2.27 Å) compared with those for Mn(2) (average 2.05 Å), while Mn(2) shows Jahn–Teller distortion in the form of an elongation of the O(23′)–Mn(2)–N(2) axis. Thus Mn(2)–O(23′) [2.201(1) Å] and Mn(2)–N(2) [2.385(1) Å] are distinctly longer than the other four bond lengths [1.877(1)–1.989(1) Å].

The coordinated water ligand is involved in intramolecular hydrogen bonding with the terminal acetate group [O(25′) ··· O(14) 2.665(2)] and is also H-bonded to an interstitial water molecule [O(14) ··· O(3) 2.793(2)]. This interstitial water molecule is H-bonded to the uncoordinated acetate ion also [O(3) ··· O(1) 2.666(3)], which is in turn H-bonded to the unbound oxygen of a type A triethanolamine ligand on a neighbouring cluster [O(2) ··· O(22′) 2.730(3)]. These H-bonds link the clusters forming a sheet-like network (Fig. 4). Full details of the hydrogen bonding are given in Table S2 (ESI †).

$[Mn_4(LH_2)_2(LH)_2(PhCO_2)_2](PhCO_2)_2\cdot CH_3CN$ (2). The asymmetric unit contains half the cluster, half an acetonitrile molecule and a benzoate ion. Mn(1) displays longer Mn–ligand

Table 1 Crystallographic data for complexes **1**, **2** and **3**

	1	**2**	**3**
Formula	$C_{32}H_{74}Mn_4N_4O_{24}$	$C_{54}H_{77}Mn_4N_5O_{20}$	$C_{30}H_{64}Mn_4N_4O_{24}Cl_2$
M_w	1118.71	1335.97	1153.49
Crystal system	Triclinic	Monoclinic	Monoclinic
Space group	$P\bar{1}$	$C2/c$	$P2_1/c$
a/Å	8.3931(1)	30.152(6)	11.2215(2)
b/Å	10.8348(1)	8.637(2)	14.7363(3)
c/Å	13.4395(1)	26.520(5)	14.8764(3)
α/°	72.638(1)	90	90
β/°	86.768(1)	119.46(3)	112.16(3)
γ/°	86.597(1)	90	90
V/Å^3	1163.46(2)	6013(2)	2278.4(8)
Z	1	4	2
D_c/g cm^{-3}	1.597	1.476	1.684
μ(Mo-Kα)/cm^{-1}	1.148	0.898	1.289
T/K	123(2)	123(2)	123(2)
λ[a]/Å	0.71073	0.71073	0.71073
Data collected	19296	32411	16110
Unique data (R_{int})	5690 (0.0482)	7039 (0.2482)	5186 (0.1139)
Observed data [$I > 2\sigma(I)$]	4755	2468	2191
Final $R1$, $wR2$[b] [$I > 2\sigma(I)$]	0.0270, 0.0654	0.0780, 0.1202	0.0702, 0.1203
(all data)	0.0377, 0.0695	0.2957, 0.1757	0.2247, 0.1587
Goodness-of-fit	1.057	0.963	0.990

[a] Graphite monochromator. [b] $R1 = \Sigma||F_o| - |F_c||/\Sigma|F_o|$, $wR2 = \{\Sigma[w(F_o^2 - F_c^2)^2]/\Sigma[w(F_o^2)^2]\}^{1/2}$.

Table 2 Selected bond distances (Å) and angles (°) for complexes **1**, **2** and **3**

1		**2**		**3**	
Mn(1)–O(13)	2.186(1)	Mn(1)–O(1)	2.281(4)	Mn(1)–O(3)	2.276(3)
Mn(1)–O(23)	2.426(1)	Mn(1)–O(7)	2.305(4)	Mn(1)–O(6)	2.288(3)
Mn(1)–O(21′)	2.128(1)	Mn(1)–O(6′)	2.083(4)	Mn(1)–O(7′)	2.108(3)
Mn(1)–O(14)	2.199(1)	Mn(1)–O(4)	2.409(5)	Mn(1)–O(5′)	2.376(4)
Mn(1)–O(11)	2.373(1)	Mn(1)–O(3)	2.308(4)	Mn(1)–O(1)	2.236(4)
Mn(1)–N(1)	2.396(1)	Mn(1)–N(1)	2.377(5)	Mn(1)–N(1)	2.383(5)
Mn(1)–O(12)	2.204(1)	Mn(1)–O(2)	2.175(4)	Mn(1)–O(2)	2.243(4)
Mn(2)–O(13)	1.877(1)	Mn(2)–O(1)	1.868(4)	Mn(2)–O(3)	1.880(4)
Mn(2)–O(23)	1.989(1)	Mn(2)–O(7)	1.962(4)	Mn(2)–O(6)	1.952(3)
Mn(2)–O(23′)	2.201(1)	Mn(2)–O(7′)	2.255(4)	Mn(2)–O(6′)	2.269(3)
Mn(2)–O(21)	1.907(1)	Mn(2)–O(6)	1.912(4)	Mn(2)–O(7)	1.910(3)
Mn(2)–O(24)	1.939(1)	Mn(2)–O(5′)	1.915(4)	Mn(2)–O(4)	1.921(4)
Mn(2)–N(2)	2.384(1)	Mn(2)–N(2)	2.316(5)	Mn(2)–N(2)	2.393(4)
Mn(1) ··· Mn(2)	3.369(3)	Mn(1) ··· Mn(2)	3.353(1)	Mn(1) ··· Mn(2)	3.205(1)
Mn(2) ··· Mn(2′)	3.222(4)	Mn(2) ··· Mn(2′)	3.165(2)	Mn(2) ··· Mn(2′)	3.187(2)
O(13)–Mn(1)–O(23)	66.77(4)	O(1)–Mn(1)–O(7)	66.31(1)	O(3)–Mn(1)–O(6)	67.13(1)
O(23)–Mn(1)–O(21′)	75.52(4)	O(7)–Mn(1)–O(6′)	76.97(1)	O(6)–Mn(1)–O(7′)	79.15(1)
O(13)–Mn(1)–O(21′)	92.02(4)	O(1)–Mn(1)–O(6′)	89.82(1)	O(3)–Mn(1)–O(7′)	91.56(1)
O(13)–Mn(2)–O(23)	82.31(4)	O(1)–Mn(2)–O(7)	81.80(2)	O(3)–Mn(2)–O(6)	82.34(2)
O(23)–Mn(2)–O(21)	96.31(5)	O(7)–Mn(2)–O(6)	92.39(2)	O(6)–Mn(2)–O(7)	92.14(2)
O(13)–Mn(2)–(23′)	82.31(4)	O(1)–Mn(2)–O(7′)	99.83(1)	O(3)–Mn(2)–O(6′)	98.84(2)
O(21)–Mn(2)–O(23′)	81.99(4)	O(6)–Mn(2)–O(7′)	81.63(1)	O(7)–Mn(2)–O(6′)	83.81(1)
O(23)–Mn(2)–O(23′)	79.59(4)	O(7)–Mn(2)–O(7′)	82.97(2)	O(6)–Mn(2)–O(6′)	82.24(1)
Mn(2)–O(21)–Mn(1′)	112.50(5)	Mn(1′)–O(6)–Mn(2)	108.66(2)	Mn(1′)–O(7)–Mn(2)	105.71(2)
Mn(2)–O(23)–Mn(2′)	100.41(4)	Mn(2)–O(7)–Mn(2′)	97.03(1)	Mn(2)–O(6)–Mn(2′)	97.76(1)
Mn(1)–O(23)–Mn(2)	99.04(4)	Mn(1)–O(7)–Mn(2)	103.32(2)	Mn(1)–O(6)–Mn(2)	103.19(2)
Mn(1)–O(23)–Mn(2′)	92.92(4)	Mn(2′)–O(7)–Mn(1)	90.78(1)	Mn(2′)–O(6)–Mn(1)	89.36(1)

bond lengths (average 2.28 Å) compared with those for Mn(2) (average 2.04 Å), while Mn(2) shows Jahn–Teller distortion in the form of an elongation of the O(7′)–Mn(2)–N(2) axis. Thus Mn(2)–O(7′) [2.256(4) Å] and Mn(2)–N(2) [2.316(5) Å] are distinctly longer than the other four bond lengths [1.868(4)–1.961(4) Å].

The uncoordinated O of the type A triethanolamine ligand is involved in hydrogen bonding to the uncoordinated benzoate ion [O(8) ··· O(9′) 2.685(7) Å] which is then hydrogen bonded to the two μ_2-O alcohol groups of a type A triethanolamine ligand in a neighbouring cluster [O(3) ··· O(10) 2.674(7) Å; O(2) ··· O(9) 2.580(1) Å]. These hydrogen bonds link the clusters into chains that run down the c axis (Fig. 5). Full details of the hydrogen bonding are given in Table S2 (ESI †).

$[Mn_4(LH_2)_2(LH)_2(EtCO_2)_2](ClO_4)_2$ (3). The asymmetric unit contains half the cluster and a perchlorate ion. Mn(1) displays longer Mn–ligand bond lengths (average 2.27 Å) compared with those for Mn(2) (average 2.05 Å), while Mn(2) shows Jahn–Teller distortion in the form of an elongation of the O(6′)–Mn(2)–N(2) axis. Thus Mn(2)–O(6′) [2.269(3) Å] and Mn(2)–N(2) [2.393(4) Å] are distinctly longer than the other four bond lengths [1.880(4)–1.952(3) Å].

The uncoordinated O of the type A triethanolamine ligand is involved in hydrogen bonding to the perchlorate ion [O(8) ··· O(12′) 2.851(6) Å] and also to a terminal O from a type B triethanolamine ligand of a neighbouring cluster [O(8) ··· O(1′) 2.666(6) Å]. These hydrogen bonds link the clusters into a sheet (Fig. 6). Full details of the hydrogen bonding are given in Table S2 (ESI †).

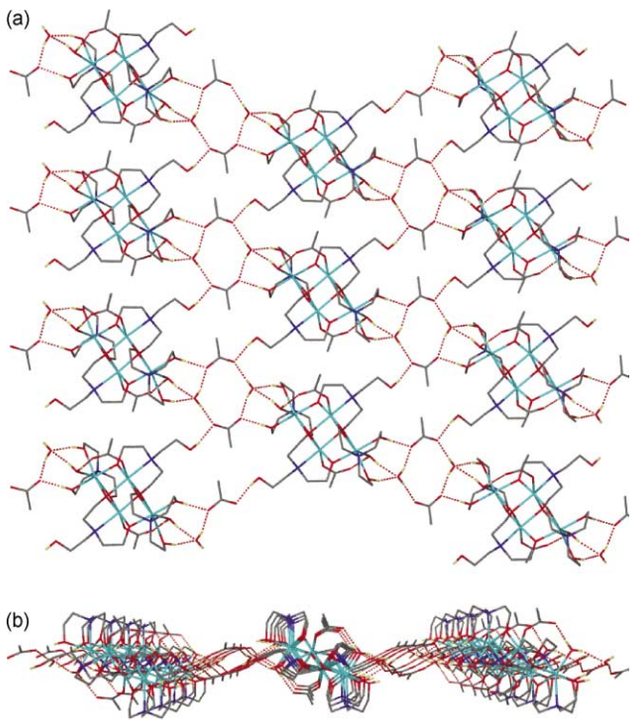

Fig. 4 The connection of clusters in **1** by H-bonding into sheet-like networks viewed perpendicular (a) and side-on (b) to the plane of the sheet.

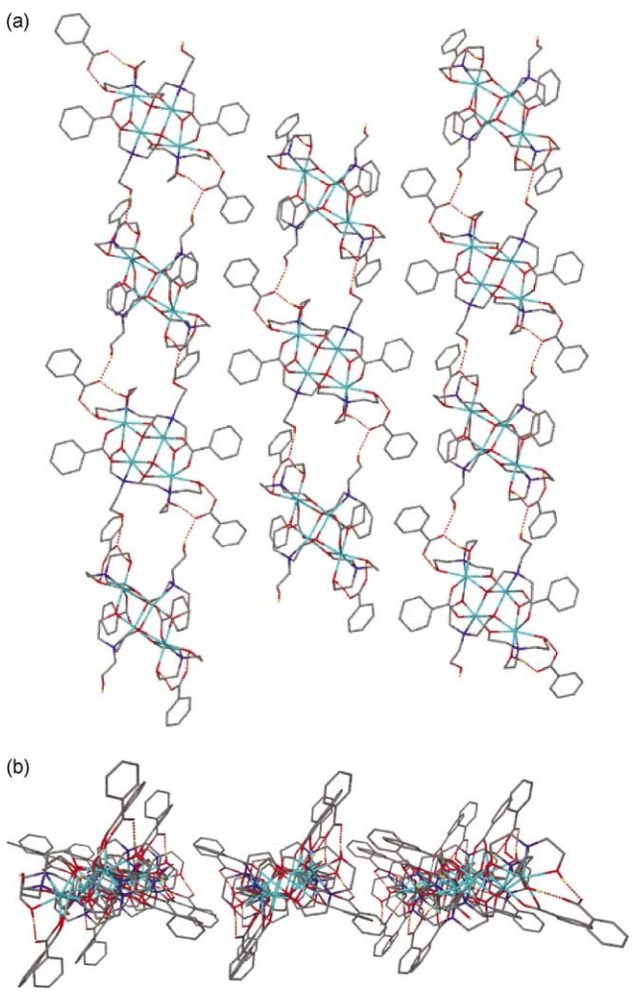

Fig. 5 Two different views of the H-bonded chains of clusters found in **2** viewed perpendicular (a) and side-on (b) to the chains.

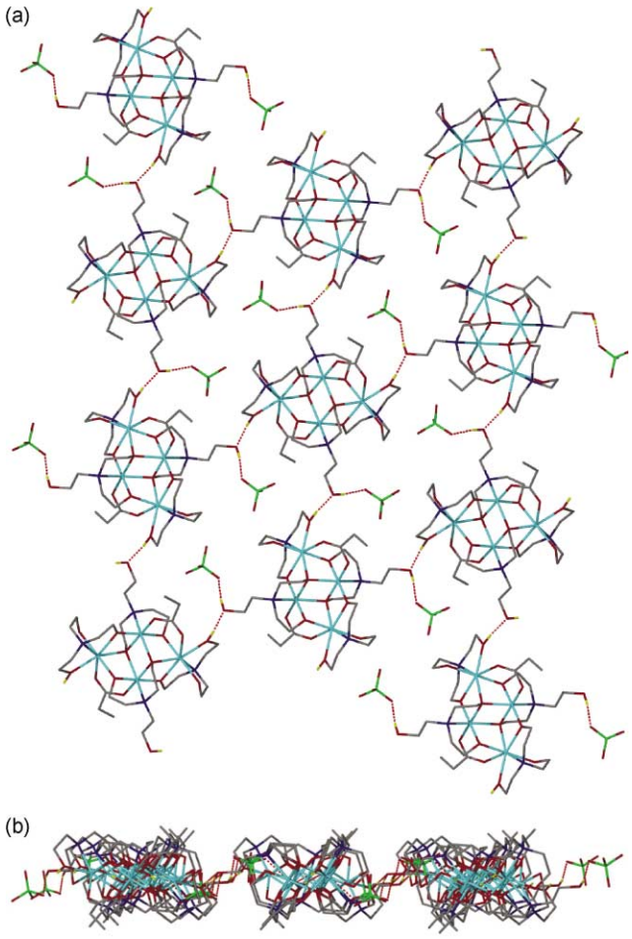

Fig. 6 The connection of clusters in **3** by H-bonding into sheet-like networks viewed perpendicular (a) and side-on (b) to the plane of the sheet.

Magnetic properties

DC magnetic susceptibilities. DC magnetic susceptibilities were measured on complexes **1** (acetate), **2** (benzoate) and **3** (propionate) in a field of 1 T, over the temperature range 300–2 K, with the powdered samples contained in a vaseline mull to prevent torquing.[19] Plots of $\chi_M T$ *versus* temperature are shown in Figs. 7 to 9. The $\chi_M T$ values for **1** and **2** increase from values typical of two Mn(II) plus two Mn(III) centres, at 300 K (~15 cm^3 mol^{-1} K), to reach a maximum of *ca.* 35.3 cm^3 mol^{-1} K (**1**) and *ca.* 26.6 cm^3 mol^{-1} K (**2**) due to intra-cluster ferromagnetic coupling, before decreasing rapidly below the temperature of the maximum, *ca.* 12 K. Similar behaviour to those of **1** and **2** has been observed by Christou, and Hendrickson *et al.*[7,8,12] on related clusters and ascribed, at low

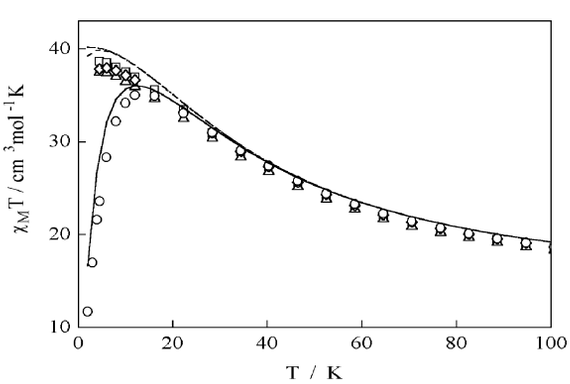

Fig. 7 Plots of $\chi_M T$ *versus* T for **1** in fields of 10000 (○), 1000 (◇), 100 (△), 20 (□) Oe. The calculated lines are for fields 10000 (—), 1000 (---), 100 (-·-), 20 (···) Oe; see text. The data are fitted well up to 300 K.

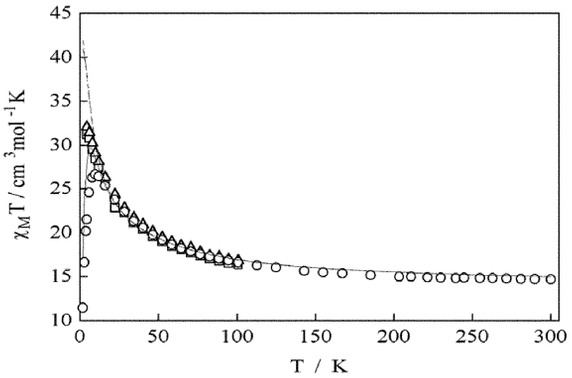

Fig. 8 Plots of $\chi_M T$ *versus* T for cluster **2** in fields of 10000 (○), 1000 (△), 100 (□) Oe. The calculated lines are for fields of 10000 (—), 1000 (- - -), 100 (-·-) Oe; see text.

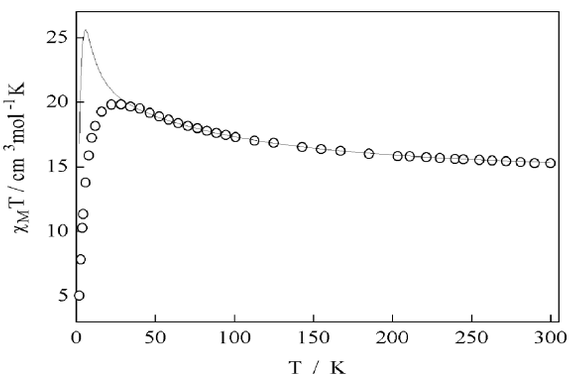

Fig. 9 Plot of $\chi_M T$ *versus* T for cluster **3** in a field of 1 T. The solid line is the calculated plot using the parameters given in the text; see reasons for the poor fit at low temperatures.

temperatures, to zero field splitting (zfs) and/or Zeeman level depopulation effects. Because of these affects, this group then restricted their fitting of such data to temperatures above the maximum in $\chi_M T$. We show, below, and in Fig. 7 that the region of the maximum can be simulated reasonably well in the case of complex **1**, by use of Van Vleck's thermodynamic form of susceptibility.[20] However, inter-cluster antiferromagnetic coupling may also be playing a part, particularly in complex **3** where a maximum in χ_M is observed at ~2.4 K under a field of 1 T. This maximum in susceptibility is not evident in **1** and **2.** While the room temperature $\chi_M T$ value for **3** is similar to those for **1** and **2**, the increase with decreasing temperature is much less marked so that the $\chi_M T$(max) value at ~28 K is lower, *viz.* 20 cm^3 mol^{-1} K, due either to different intra-cluster exchange interactions and/or the stronger inter-cluster antiferromagnetic coupling noted in the χ_M data, as well as zfs.

To deduce the intra-cluster J values we have employed the same Heisenberg–Van Vleck model as that used by Christou, and Hendrickson *et al.*[7,8] The atom numbering and exchange parameters are shown in Fig. 10. The spin Hamiltonian used and details of the Kambe approach for this 2;5/2;2;5/2 spin system of Mn1 ··· Mn4 are as given by Christou *et al.*[7,8]

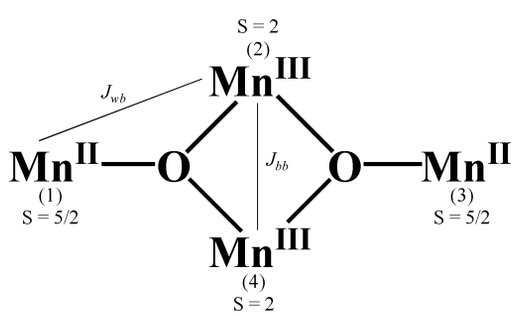

Fig. 10 Atom numbering and exchange coupling scheme.

However, the thermodynamic susceptibility expression has been employed here, as indicated above.

The $\mathscr{H} = \Sigma -2J_{ij}\boldsymbol{S}_i \cdot \boldsymbol{S}_j$ type Hamiltonian for a tetranuclear assembly[20] is transformed into eqn. (1), where the interaction between the two manganese centres Mn1 and Mn3, J_{ww}, is assumed to be negligible.

$$\mathscr{H} = -J_{wb}(\boldsymbol{S}_T^2 - \boldsymbol{S}_A^2 - \boldsymbol{S}_B^2) - J_{bb}(\boldsymbol{S}_A^2 - \boldsymbol{S}_1^2 - \boldsymbol{S}_3^2) \quad (1)$$

$$\text{where } \boldsymbol{S}_A = \boldsymbol{S}_1 + \boldsymbol{S}_3 \quad \boldsymbol{S}_B = \boldsymbol{S}_2 + \boldsymbol{S}_4 \quad \boldsymbol{S}_T = \boldsymbol{S}_A + \boldsymbol{S}_B \quad (2)$$

The Kambe equivalent operator method gives the energy expression in eqn. (3)

$$E(S_T) = -J_{wb}[S_T(S_T + 1) - S_A(S_A + 1) - S_B(S_B + 1)] - J_{bb}[S_A(S_A + 1)] \quad (3)$$

There are 110 possible states with S_T (total spin) for the cluster ranging from 0 to 9. The energies of these S_T states are incorporated in to the Van Vleck thermodynamic expression for susceptibility.[7,20]

We also carried out variable field measurements in the $\chi_M T$ maximum region, which, in the case of **1** and **2**, for example, does not lead to the rapid turnover when fields of 0.1 T, 0.01 T and 0.002 T are employed, compared to the kind noted at 1 T (Figs. 7 and 8). Although there are some discrepancies between the calculated and observed $\chi_M T$ values of **1** in the 0.1 to 0.002 T fields, the trends are correct and the plots for these different field values could be simulated with the parameter combination used for the 1 T data. This indicates that, while the region 20–300 K is best represented by the model, Zeeman level population effects are probably as important as zero field splitting (D) effects, the latter not being included in the spin Hamiltonian of eqn. (1).

For complex **2**, the $\chi_M T$ values above the maximum are independent of field (1.0, 0.1 and 0.01 T). The best fit parameters used to simulate the region 16 K to 300 K reproduce the region of maximum and below reasonably well, the calculated value of $\chi_M T$(max) being a bit higher (29.7 cm^3 mol^{-1} K) than the observed. The observed data in the range 2–16 K are lower than the values calculated using the parameters used to fit the higher temperatures in fields of 0.1 and 0.01 T but, again, the trend of no maximum is evident (Fig. 8). In the case of **3**, the observed $\chi_M T$ values are essentially independent of applied field (0.01, 0.1 and 1 T) between 300 and 2 K. The region of $\chi_M T$(max), below ~40 K, could not be simulated by use of Hamiltonian (1) but the data were well reproduced above 40 K (Fig. 9). Further comments are given below.

The best-fit parameter values are now given. J_{bb} is the coupling between the 'body' Mn(III) ($S = 2$) ions and J_{wb} is the coupling between the Mn(II) ($S = 5/2$) 'wing' and the Mn(III) ions (Fig. 11). J_{ww}, the coupling between the Mn(II) centres, is assumed to be zero.

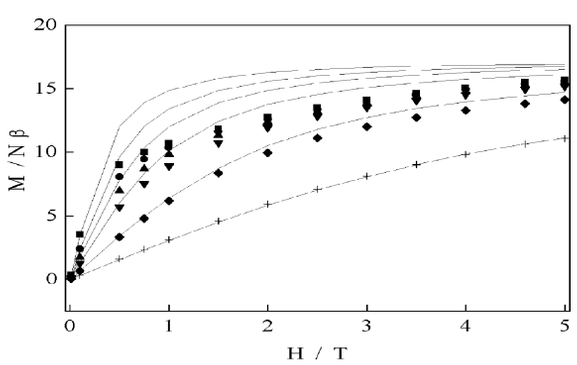

Fig. 11 Magnetization isotherms for **1** at temperatures 20 (+), 10 (◆), 5.5 (▼), 4 (▲), 3 (●), 2 K (■). The solid lines are those calculated using the tetramer model with the g and J values given in the text, for 20 K (bottom) to 2 K (top).

Complex **1**; $g = 1.89$, $J_{bb} = 6.5$ cm^{-1}, $J_{wb} = 1.7$ cm^{-1}.

This combination gives the total spin level, $S_T = 9$, an energy of zero and the next level $S_T = 8$ is close by at 13.6 cm^{-1}. The ground state has S_T, S_A and S_B values of 9, 4 and 5.

Complex **2**; $g = 1.95$, $J_{bb} = 6.6$ cm^{-1}, $J_{wb} = 0.4$ cm^{-1}.

The $S_T = 8$ level is only 3.3 cm^{-1} above the ground $S_T = 9$ and sixteen other S_T levels are within 20 cm^{-1}.

Complex **3**; $g = 1.95$, $J_{bb} = 10.9$ cm^{-1}, $J_{wb} = 0.22$ cm^{-1} (data were fitted at temperatures above $\chi_M T$(max)).

The $S_T = 8$ level is only 1.8 cm^{-1} above the ground $S_T = 9$ for complex **3**. Seventeen S_T levels with S_T values 3 to 8 are within 11 cm^{-1} of the ground level.

Use of a negative, rather than positive J_{bb} in **3** did cause the $\chi_M T$ values to decrease, below 50 K, but the maximum in $\chi_M T$ that is observed at ~ 28 K was not reproduced. Thus, the low temperature behaviour for **3** is likely to arise from very weak inter-cluster coupling. Indeed, as a rough approximation, we used a J between neighbouring $S = 9$ clusters of -0.04 cm^{-1}, in a trimer of clusters model, and obtained the kind of decrease in $\chi_M T$ observed below 28 K. A detailed analysis of the inter-cluster Mn ··· Mn and H-bonding distances in **1** to **3** indicates that it is probably the way the cluster links together that gives rise to antiferromagnetic inter-cluster coupling in **3**. Each cluster in **3** is joined directly to four neighbouring clusters *via* a H-bond between the uncoordinated arm (O(8)) of a type A ligand and a terminal arm of a type B ligand (O(1)H). In **1** and **2** the clusters are linked indirectly *via* H-bonding to the carboxylate anion (and H_2O in **1**).

The abovementioned g, J_{bb}, and J_{wb} values, for **1** and **2**, are of similar magnitude to those found by Christou, and Hendrickson *et al.*[7,8,12] for related alkoxo-carboxylato bridged clusters most of which have $S_T = 9$ ground states, except for one having $S_T = 8$.[8] The values for **3** are somewhat different, having a lower value of J_{wb} and higher J_{bb} compared to **1** and **2**. Further discussion of S_T values is given in regard to the magnetization isotherm data and fitting. In general, the 'outer' bridging groups such as carboxylate, triethanolamine and hydroxymethylpyridines[7,8,12] do not play a major role in determining the size of the J coupling constants. The 'core' structure is the dominant factor.

DC magnetization *versus* magnetic field studies. Magnetization isotherms (2 to 20 K; fields 0 to 5 T) were obtained on samples of **1** to **3** which were dispersed in vaseline mulls to prevent crystallite orientation anomalies (torquing).[19] These data were analysed in order to attempt to unambiguously determine the ground spin state, the size and sign of the zfs D term, and perhaps provide information on any coupling between the Mn_4 clusters.

The magnetization isotherms at 2, 3, 4, 5.5, 10 and 20 K for cluster **1** are shown in Fig. 11. It can be seen that saturation does not occur in the highest fields even at 2 K, thus indicating that the ground state is not isolated energetically from higher states and/or is split by some other interaction such as zero field splitting. This is in agreement with the susceptibility analysis. The 2 to 4 K magnetizations become very similar in size above 2 T and reach ~15.5 Nβ at $H = 5$ T, below the value of 17 Nβ expected for an isolated $S_T = 9$ state, with a $g = 1.89$. The 0 to 1 T region of Fig. 11 was investigated in more detail and gradual curvature was observed in the 2 to 5.5 K isotherms (not shown). This low field region also gave no evidence for any antiferromagnetic ordering transition, down to 2 K, of the type recently observed for a Mn_4–hmp analogue.[11,12] There was no S-shaped behaviour in the M *vs.* ±2000 Oe plot typical of a metamagnetic transition. Thus any intercluster interactions are extremely weak in **1**. Included in Fig. 11 are the calculated M values using the g, J_{bb} and J_{wb} parameters obtained for the 1 T field data analysed using the tetramer model of eqns. (1) to (3). It can be seen that the 20 K data fit very well while, below 5.5 K, the low field region is fitted quite well whereas the higher fields give calculated values well above the observed data. This is because of zero field splitting and other effects, not included in the tetramer model.

Calculations of magnetisation were made at the lowest temperature, 2 K, to avoid the influence of excited spin states, using powder averaging methods[20] and the Hamiltonion for an isolated ground state given in eqn. (4).

$$\mathcal{H} = D\boldsymbol{S}_z^2 + g\beta\boldsymbol{H}\cdot\boldsymbol{S} \qquad (4)$$

The best-fit for **1**, for a $S = 9$ state, with D assumed negative in view of the two parallel Jahn–Teller elongated Mn(III) axes and the frequency dependent AC χ'' data, is $g = 1.89$ and $D = -0.21$ cm^{-1}. However, as shown in Fig. 12, while this gave a great improvement, compared to using the tetramer model ($D = 0$), it underestimated the observed values at low fields (*e.g.* 1 T) and overestimated them at high fields (*e.g.* 5 T). Interestingly, use of a positive D, with $g = 1.89$ and $D = +0.30$ cm^{-1}, gave better agreement at most fields. A similar situation occurs for **2** but the values $g = 1.95$ and $D = -0.23$ cm^{-1} were preferable in that case (see below and Fig. 13). This dilemma encouraged us to explore these calculations further, since the M values are very sensitive to field induced splittings of the energy levels, particularly in the perpendicular direction.[21] M values are given in Fig. 13 for D varying between -1 to $+1$ cm^{-1}, with $g = 1.89$, at 2 K. The values of M observed, given as horizontal lines for **1**, provide better agreement for D negative, at $H = 1$ T, and 'track' more sensibly at higher fields. Use of an isolated $S = 8$ state, rather than $S = 9$, while not in agreement with the tetramer model fitting analysis (eqns. (1)–(3)), also gave poor agreement with the magnetisation data of **1** and **2**. High field EPR measurements[7,8] would be useful to confirm the sign and size of D.

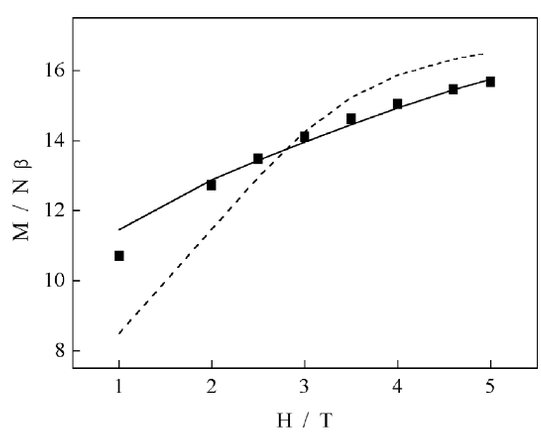

Fig. 12 Plots of magnetization (■) *versus* field (1–5 T), at 2 K, for **1**. The dashed line is that calculated for $g = 1.89$ and $D = -0.21$ cm^{-1}. The solid line is that calculated using $g = 1.89$ and $D = +0.30$ cm^{-1}.

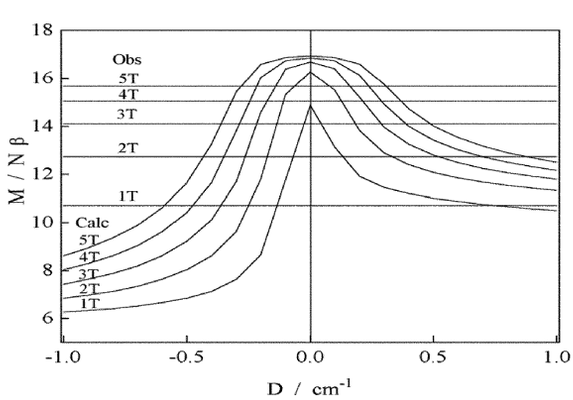

Fig. 13 Calculated M values at 2 K using $g = 1.89$ and D positive and negative (the curves should be smooth). Horizontal lines are the M values observed in the fields given.

The magnetisation data were also plotted as isofield 1, 2, 3, 4 and 5 T curves, in the *M vs. H*/*T* manner presented by Christou, and Hendrickson *et al.*[7,8,12] (See Figs. S1 and S2 in ESI†). The non-superimposed isofield data clearly show that zero field splitting is occuring. Fitting of the *M vs. H*/*T* data do not yield any new information to that discussed above and suffer from the possible effects of excited states especially at 4 K. Similar qualities of fits to those discussed here have recently been obtained by Christou *et al.*[22] for a {$Mn^{II}_4Mn^{III}_3$–hmp} cluster and ascribed to the influence of low lying excited states, even at temperatures of 1.8–4 K. The possibility of a positive *D* was not discussed for this non-SMM cluster. Weak cluster–cluster H-bonding interactions were evident down to 0.04 K. Such behavior is different in detail to the structurally similar Mn_7–triethanolamine cluster mentioned earlier.[17]

The *M*/*H* data for the propionate cluster **3** are different in detail to those for **1** and **2**. This is a result of the intercluster antiferromagnetic coupling noted in the χ_M data at very low temperatures. Thus, the *M* values, in fields of less than 2 T, are essentially a linear function of *H*, and much lower in magnitude at a particular *H* than for **1** and **2**. The *M* value, at 2 K and 5 T, is similar to those of **1** and **2** (*ca.* 16 Nβ) and is still increasing rapidly, thus being far from a saturation value in this high field/low temperature region. There is a gentle S-shape in the 2 K data below 2 T, perhaps indicative of antiferromagnetic to metamagnetic behaviour arising from intercluster interactions. Indeed, plots of *M vs. T* for fields of 0.01, 0.1, 0.5, 0.75, 1.0 and 1.5 T, show maxima in *M* at 2.5 K in fields above 0.5 T, indicative of antiferromagnetic coupling (Fig. 14). Heat capacity measurements would be required to see if this is an antiferromagnetic phase transition as was observed in $[Mn_4(hmp)_6Br_2(H_2O)_2]Br_2$.[11] To date, we have not achieved any satisfactory quantitative analysis of the magnetization data obtained on **3**.

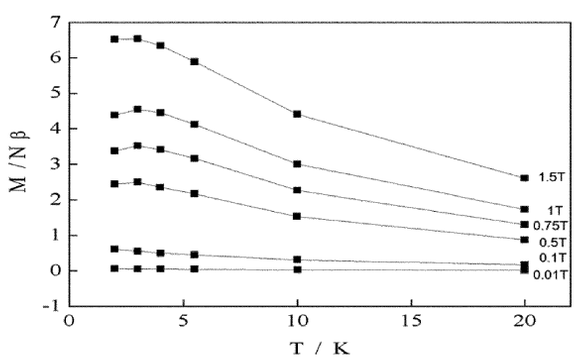

Fig. 14 Observed *M* values for cluster **3** in the fields given. The solid lines just join the points.

AC magnetic susceptibilities

These measurements, made as a function of AC field oscillation frequency, provide strong evidence that **1** and **2** are SMMs as was the case in related hmp and pdmH $Mn^{II/III}_4$ clusters.[7,8] Plots of χ'_M and χ''_M *versus T* are given for **1** in Fig. 15. Those for **2** are very similar and both show that there is no problem with a distribution of relaxation times.[5] Maxima in χ''_M occur, for these different frequencies, in the temperature range 2.5 K to 1.5 K. The magnetization relaxation data were analysed using the Arrhenius law $\tau = \tau_0\exp(-\Delta E/k_BT)$, where τ is the relaxation time, ΔE is the activation energy, k_B is the Boltzmann constant and τ_o is the preexponential factor. A plot of $\ln(1/\tau)$ *vs.* $1/T$ for **1** gave a linear dependence which was least-squares fitted to the Arrhenius equation to yield $\Delta E = 22.4$ K and $\tau_0 = 5.12 \times 10^{-8}$ s. Likewise, for **2**, the best fit yielded $\Delta E = 20.3$ K and $\tau_0 = 1.56 \times 10^{-7}$ s. These ΔE and τ_0 values are similar to those obtained for the tetranuclear hmp and pdmH

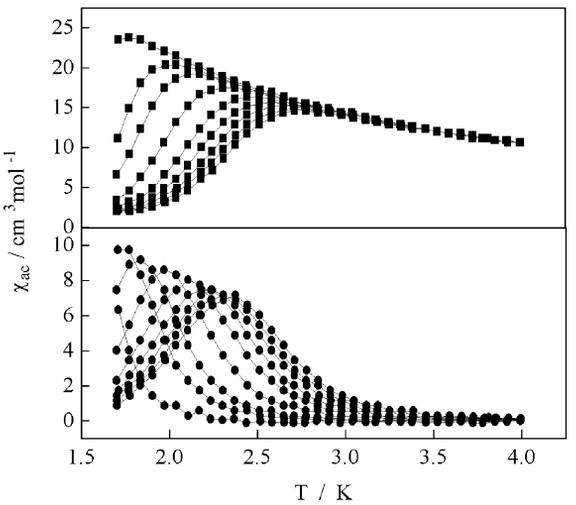

Fig. 15 AC susceptibilities for **1**. Top: χ'_M values for frequencies, right to left, 1500, 1250, 1000, 750, 500, 100, 50, 10 Hz. Bottom: χ''_M values for the same frequencies, right to left, clearly showing the maxima.

analogues[7,8] and for a heptanuclear triethanolamine $Mn^{II}_4Mn^{III}_3$ cluster, the latter having $S = 11$.[17] The ΔE value for **1** can be compared to the potential energy barrier for magnetization reversal[4,5,8] calculated from $U = |DS_z^2|$ using the DC *M*/*H* data, with $D = -0.21$ cm^{-1} and $S_z = 9$, *viz.* 24.5 K. (The $D = +0.32$ cm^{-1} value would give poorer agreement between *U* and ΔE.) The *U* value for **2** is 26.8 K. The ΔE and *U* values are not expected to be equal and, as in related systems, *U* was found to be greater than ΔE.[4,5,8]

In the case of the propionate cluster, **3**, the AC χ''_M measurements shown in Fig. 16 display a frequency dependence but do not yield maxima down to 1.7 K, even at the highest frequency used (1500 Hz). Maxima are likely below this temperature thus indicating SMM behaviour is also occurring for **3**. The difference in the temperature of the peaks compared to those of **1** and **2**, and the low values of χ''_M in **3**, probably reflect the intercluster antiferromagnetic coupling noted in DC susceptibilities for the latter. The χ'_M *versus T* plot is also different to those of **1** and **2** again reflecting the antiferromagnetic contribution. Frequency dependent χ''_M plots rather similar to those of **3** have recently been reported for $[Mn_4(hmp)_6(acac)_2(MeO)_2](ClO_4)_2$·2MeOH and related analogues, although their DC χ_MT *versus* temperature behaviour, and best-fit *g* and *J* values are much more akin to those of **1** and **2**.[12]

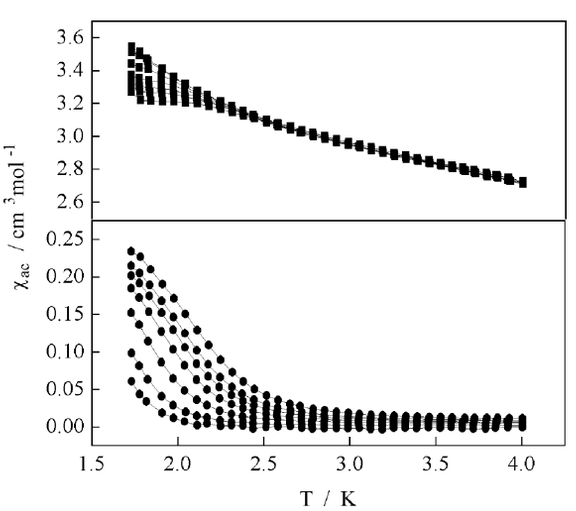

Fig. 16 AC susceptibilities for **3**. Top: χ'_M values for frequencies, bottom to top, 1500, 1250, 1000, 750, 500, 100, 50 Hz. Bottom: χ''_M values for the same frequencies, right to left.

Summary

This new family of triethanolamine capped $Mn^{II}_2Mn^{III}_2$–carboxylate SMMs complements a known heptanuclear $Mn^{II}_4Mn^{III}_3$ derivative[17] and a range of related tetranuclear pyridyl–alcohol analogues.[7,8] The ground state spin, $S = 9$, the nearby energy levels and the relaxation effects induced by magnetization reversal have been probed in detail by DC and AC magnetic measurements. Limitations on the analysis of the axial zero field splitting term, D, using high field DC magnetization data for such systems, have been emphasized. A particular structural feature of these rhomboidal clusters is the way that non-coordinated alcohol groups on the triethanolamine ligands are used to link the clusters together, *via* hydrogen-bonding, into extended networks of 1D or 2D topology. Interestingly, these inter-cluster effects are too weak, electronically, in the acetate and benzoate clusters to influence SMM properties. They do, however, lead to inter-cluster antiferromagnetic coupling in the propionate case and to χ''_M maxima, in the out-of-phase AC susceptibilities, occurring at significantly lower temperatures than in the acetate and benzoate clusters. Related intermolecular interactions have been noted in Mn^{III}_4 Schiff-base clusters.[23]

Acknowledgements

Grants from the Australian Research Council (ARC) to K. S. M. (Discovery grant) and to S. R. B. (Australian Research Fellowship), and from Monash University Special Research Funds (to L. S, K. S. M. and L. W.) are gratefully acknowledged.

References

1 P. Jensen, S. R. Batten, B. Moubaraki and K. S. Murray, unpublished data.
2 D. J. Price, S. R. Batten, K. J. Berry, B. Moubaraki and K. S. Murray, *Polyhedron*, 2003, **22**, 165.
3 D. J. Price, S. R. Batten, B. Moubaraki and K. S. Murray, *Chem. Commun.*, 2002, 762.
4 D. N. Hendrickson, G. Christou, H. Hishimoto, J. Yoo, E. K. Brechin, A. Yamaguchi, E. M. Rumberger, S. M. J. Aubin, Z. Sun and G. Aromi, *Polyhedron*, 2001, **20**, 1479.
5 D. Gatteschi and R. Sessoli, *Angew. Chem., Int. Ed.*, 2003, **42**, 268.
6 L. Wittick, S. R. Batten, B. Moubaraki, K. S. Murray and L. Spiccia, unpublished data.
7 J. Yoo, A. Yamaguchi, M. Nakano, J. Krzystek, W. E. Streib, L-C. Brunel, H. Ishimoto, G. Christou and D. N. Hendrickson, *Inorg. Chem.*, 2001, **40**, 4604.
8 J. Yoo, E. K. Brechin, A. Yamaguchi, M. Nakano, J. C. Huffman, A. L. Maniero, L-C. Brunel, K. Awaga, H. Ishimoto, G. Christou and D. N. Christou, *Inorg. Chem.*, 2000, **39**, 3615.
9 E. K. Brechin, M. Soler, J. Davidson, S. Parsons and G. Christou, *Chem. Commun.*, 2002, 2252.
10 A. Battacharjee, Y. Myazaki, M. Nakano, J. Yoo, G. Christou, D. N Hendrickson and M. Sorai, *Polyhedron*, 2001, **20**, 1607.
11 A. Yamaguchi, N. Kusumi, H. Ishimoto, H. Mitamura, T. Goto, N. Mori, M. Nakano, K. Awaga, J. Yoo, D. N. Hendrickson and G. Christou, *J. Phys. Soc. Jpn.*, 2002, **71**, 414.
12 E-C. Yang, N. Harden, W. Wernsdorfer, L. Zakharov, E. K. Brechin, A. L. Rheingold, G. Christou and D. N. Hendrickson, *Polyhedron*, 2003, **22**, 1857.
13 J. B. Vincent, H-R. Chang, K. Folting, J. C. Huffman, G. Christou and D. N. Hendrickson, *J. Am. Chem. Soc.*, 1987, **109**, 5703.
14 J. B. Vincent, C. Christmas, H-R. Chang, Q. Li, P. Boyd, J. C. Huffman, D. N. Hendrickson and G. Christou, *J. Am. Chem. Soc.*, 1989, **111**, 2086.
15 Z. Otwinowski and W. Minor, *Methods Enzymol.*, 1996, **276**, 307.
16 G. M. Sheldrick, SHELXL-97, Program for refinement of crystal structures, University of Göttingen, Germany, 1997.
17 B. Pilawa, M. Keleman, S. Wanka, A. Geisselmann and A. Barra, *Europhys. Lett.*, 1998, **43**, 7.
18 H. H. Thorp, *Inorg. Chem.*, 1992, **31**, 1585.
19 B. J. Kennedy and K. S. Murray, *Inorg.Chem.*, 1985, **24**, 1552.
20 K. S. Murray, *Adv. Inorg. Chem.*, 1995, **43**, 261.
21 G. Harris, *J. Chem. Phys.*, 1968, **48**, 2191.
22 N. C. Harden, M. A. Bolcar, W. Wernsdorfer, K. A. Abboud, W. E. Streib and G. Christou, *Inorg. Chem.*, 2003, **42**, 7067.
23 C. Boskovic, R. Bircher, P. L. W. Tregenna-Piggott, H. A. Güdel, C. Paulsen, W. Wernsdorfer, A.-L. Barra, E. Khatsko, A. Neels and H. Stoeckli-Evans, *J. Am. Chem. Soc.*, 2003, **125**, 14046.
24 H. Miyasaka, K. Nakata, K. Sugiura, M. Yamashita and R. Clerac, *Angew. Chem., Int. Ed.*, 2004, **43**, 707.
25 M. Murugesu, K. A. Abboud and G. Christou, *Dalton Trans.*, 2003, 4552.